Ultrafast photoreduction dynamics of a new class of CPD photolyases

Fabien Lacombat, Agathe Espagne, Nadia Dozova, Pascal Plaza, Pavel Müller, Hans-Joachim Emmerich, Martin Saft, Lars-Oliver Essen

Ultrafast Photoreduction Dynamics of a New Class of CPD Photolyases

Fabien Lacombat,[a] Agathe Espagne,[a] Nadia Dozova,[a] Pascal Plaza,*[,a] Pavel Müller,*[,b] Hans-Joachim Emmerich,[c] Martin Saft,[c] Lars-Oliver Essen*[,c]

[a] *PASTEUR, Département de chimie, École normale supérieure, PSL University, Sorbonne Université, CNRS, 75005 Paris, France. E-mail: pascal.plaza@ens.fr*

[b] *Université Paris-Saclay, CEA, CNRS, Institute for Integrative Biology of the Cell (I2BC), 91198, Gif-sur-Yvette, France. E-mail: pavel.muller@i2bc.paris-saclay.fr*

[c] *Department of Chemistry, Center for Synthetic Microbiology, Philipps University, 35032 Marburg, Germany. E-mail: essen@chemie.uni-marburg.de*

KEYWORDS:

CPD photolyase, photoactivation, photoreduction, electron transfer, flavin, tryptophan, deprotonation, ultrafast, transient absorption, spectroscopy, anisotropy

ABSTRACT:

NewPHL is a recently discovered subgroup of ancestral DNA photolyases. Its domain architecture displays pronounced differences from that of canonical photolyases, in particular at the level of the characteristic electron transfer chain, which is limited to merely two tryptophans, instead of the "classical" three or four. Using transient absorption spectroscopy, we show that the dynamics of photoreduction of the oxidized FAD cofactor in the NewPHL begins similarly as that in canonical photolyases, *i.e.*, with a sub-ps primary reduction of the excited FAD cofactor by an adjacent tryptophan, followed by migration of the electron hole towards the second tryptophan in the tens of ps regime. However, the resulting tryptophanyl radical then undergoes an unprecedentedly fast deprotonation in less than 100 ps in the NewPHL. In spite of the stabilization effect of this deprotonation, almost complete charge recombination follows in two phases of ~950 ps and ~50 ns. Such a rapid recombination of the radical pair implies that the first FAD photoreduction step, *i.e.*, conversion of the fully oxidized to the semi-quinone state, should be rather difficult *in vivo*. We hence suggest that the flavin chromophore

likely switches only between its semi-reduced and fully reduced form in NewPHL under physiological conditions.

FOREWORD:

This article is dedicated to Klaus Brettel on the occasion of his retirement. Klaus has played a major role in the careers of several authors of the present article. Mentor and dear friend for some of us, close collaborator for others, he has guided us and provided us with the example of research of the highest scientific level, conducted with unfailing rigor, most discerning standards and absolute honesty.

MANUSCRIPT TEXT:

1. INTRODUCTION

Photolyases and cryptochromes form a superfamily (PCSf) of structurally related flavoproteins, which mediate with their non-covalently bound flavin adenine dicluneotide (FAD) numerous light-dependent functions in organisms of all kingdoms of Life [1]. Photolyases are enzymes specialized in repairing UV-damaged DNA [2], *i.e.* pyrimidine dimer lesions, using visible light [1,3-6]. Cryptochromes are blue-light photoreceptors triggering biological responses as diverse as photomorphogenesis of plants, entrainment of circadian rhythms and possibly photomagnetoreception in a number of migrating species [1,7-11].

Understanding the primary reaction mechanisms of these proteins at the molecular level has been the subject of a plethora of biological, biophysical and theoretical studies, in particular by time-resolved spectroscopic techniques, since the early works of A. Sancar and collaborators on *E. coli* photolyase (*Ec*CPD) in the 1980's [12-14]. One photoinduced reaction has been particularly scrutinized, namely the process called photoactivation, by which the flavin cofactor of photolyases is photoreduced from the oxidized (FAD_{ox}) or semi-reduced ($FADH^{\bullet}$) states to the enzymatically-active, fully reduced state ($FADH^{-}$) [1,5]. The first photoreduction step (FAD_{ox} to $FAD^{\bullet-}/FADH^{\bullet}$) is also believed to trigger the signaling process of cryptochromes [9]. Aubert *et al.* have demonstrated for the first time [15] that flavin photoreduction in microbial class I CPD photolyases occurs in a stepwise manner via a chain of three conserved tryptophan (Trp) residues, connecting the deeply buried flavin to the protein surface [16]. Upon photoexcitation, the flavin abstracts an electron from the first, proximal Trp (in a fraction of a ps for FAD_{ox} [17] and in a few tens of ps for $FADH^{\bullet}$ [18,19]), producing the cationic tryptophanyl radical

(noted $TrpH^{\bullet+}$). Migration of the electron hole along the Trp triad then follows in the tens to hundreds of ps [17-19]. Once the third, distal Trp is oxidized, it deprotonates in a few hundreds of ns, producing the neutral tryptophanyl radical ($Trp^{\bullet}$). This considerably slows down charge recombination, to the ms timescale [18,20], and leaves enough time for external reductants (thiols [14] or NAD(P)H [21,22]) to quench the tryptophanyl radical, thereby stabilizing the reduced flavin. Similar patterns, involving the so-called "canonical" Trp triad, were found in the photolyases of other types of organisms [23,24], as well as in cryptochromes [23-25]. However, a growing number of alternative electron transfer (ET) pathways have also been reported in different members of the PCSf. These include a non-canonical third Trp as final electron donor [25,26], the hypothetical role of an aspartate (Asp) as a stepping stone between Trp's [27], the involvement of tyrosine (Tyr) residues as final or alternative donors [28-32], the absence of canonical proximal Trp [31]. the presence of a completely different Trp triad [33-35], branched Trp chains [36], or the existence of a fourth distal donor (Trp or Tyr) in the ET chain [32,37-39].

In this work, we examine the unusual photoreduction chain of a new non-canonical subgroup of the PCSf, coined NewPHL, that was recently discovered by a bioinformatic approach [40]. The NewPHL subgroup is relatively small, 632 sequences with sequence lengths of 255 to 484 amino acids, and its host organisms are mostly bacteria from a marine habitat. The domain architecture of NewPHLs exhibit pronounced differences from that of other PCSf members, at both the levels of the catalytic FAD-binding domain and the C-terminal extension. Based on a homology model (Figure 1) [40], it moreover appears that the canonical Trp triad is not fully evolved in NewPHL, the distal Trp being notably absent in this ancestral photolyase. This unusual configuration raises questions as to how the protein sustains the photoreduction activity reported *in vitro* by Emmerich *et al.,* for both oxidized and semi-reduced forms of the enzyme, in the presence of 50 mM dithiothreitol (DTT) as reducing agent [40]. Indeed, in the W306F mutant of *Ec*CPD, where the distal Trp was replaced by a redox-inert phenylalanine (Phe), the photoreduction of $FADH^{\bullet}$ was reported to be abolished *in vitro* (25 mM DTT) [41]. Transient absorption studies performed on this mutant showed that charge recombination following the initial photoinduced charge separation was highly accelerated in the absence of external reductant. Starting from the semi-reduced state of the flavin, charge recombination was reported to occur in ~1 µs [42], *i.e.* four orders of magnitude faster than in wild-type (WT) *Ec*CPD [43]. This type of effect, in similar proportions, was reported after replacing the fourth Trp of an animal (6-4) photolyase by a Phe [37,44].

Here, we specifically dwell on the NewPHL from *Dinoroseobacter shibae* (*Ds*NewPHL), a facultative anaerobic and anoxygenic photoheterotroph. Our scope focuses on the first FAD photoreduction step in

*Ds*NewPHL, which we studied by a combination of transient absorption spectroscopic techniques covering timescales from hundred femtoseconds to microseconds.

2. MATERIALS AND METHODS

2.1. Sample preparation of *Ds*NewPHL

The *Dinoroseobacter shibae* NewPHL (*Ds*NewPHL) was prepared by recombinant overproduction in *E. coli* as previously reported [40]. Under standard aerobic conditions, the protein elutes in its semi-reduced form with its UV-Vis spectrum exhibiting the typical broad red band of $FADH^{\bullet}$ [40]. The oxidized form of the protein was obtained by overnight incubation in the presence of potassium ferricyanide. The UV-Vis spectrum of DsNewPHL then shows the characteristic bands of FAD_{ox} [45], peaking here at 374 and 444 nm (see Figure S1 in Supplementary Information (SI), Section S1) [40]. Based on the ratio of the sample absorbance at 280 nm (protein+FAD_{ox}) and 444 nm (FAD_{ox} alone), we estimated that the protein/flavin ratio is close to 1. Concentration over spin filters (Amicon Ultra-4, 30 kDa cutoff) for femtosecond transient absorption measurements, as well as freezing and thawing, however induces moderate losses (≤15%) of bound flavin.

The working buffer composition was: 50 mM phosphate at pH 8.0, 100 mM NaCl, 20% glycerol. D_2O buffer was prepared by exchange with heavy water (99.9 atom % D, Sigma-Aldrich) as previously described [32,34].

2.2. Femtosecond transient absorption spectroscopy (TAS)

2.2.1. Experimental conditions

Polarized transient absorption spectra were recorded by the pump-probe technique, with a white-light continuum probe, as previously described [32,34,39,46]. The pump pulses (70 fs) were tuned at 470 nm by using a two-stage non-collinear optical parametric amplifier (NOPA, Clark MXR). The energy used to excite the samples was ~0.1 µJ per pulse, focused on a surface of ~6100 µm² (at half of maximum). The fraction of excited molecules in the probed volume was estimated to ~5-6% by calculation based on sample absorbance, pump energy and pump/probe transverse profiles [47], as well as comparison with a reference sample of tris-(2,2'-bipyridyl)-ruthenium(II) complex [48,49].

The *Ds*NewPHL samples were kept at 5 °C during the experiments with the help of a circulating thermostatic bath. Steady-state absorption spectra of the samples were regularly recorded during the experiments to check that no substantial degradation occurred. The samples, concentrated to ~140 µM

FAD_{ox} (see SI, Section S1), were held in 1-mm-path fused silica cells (FireflySci), continuously moving in two dimensions to avoid consecutive irradiation of the same volume [39].

The polarized differential absorptions ($\Delta A_{\parallel}$ and $\Delta A_{\perp}$, not shown) were first corrected from the chirp of the probe beam, independently measured by recording cross-phase modulation [50] (XPM) in the pure solvent. They were then used to calculate the isotropic transient absorptions (ΔA_{iso}) and transient anisotropy (*r*) using the standard definitions of these quantities [32,34,39]. Note that rotational diffusion of *Ds*NewPHL as a whole is not expected to play any role in the anisotropy dynamics during the time 3.2 ns window of our measurements. Indeed, previous reports showed that the rotational diffusion time (τ_{rot}) of other photolyases under comparable conditions is of the order several tens of ns (depending on glycerol content and temperature) [39,51]. Given that the size of *Ds*NewPHL (47 kDa) is somewhat smaller than that of standard photolyases (~55-60 kDa), a small correction should be applied to the literature data (factor of at most ~0.8) but without changing the order of magnitude. The anisotropy dynamics presented below should thus be considered as characteristic of intrinsic changes within the protein.

2.2.2. Kinetic analysis

The ultrafast transient absorption data were globally fitted [52] to a sum of exponential functions, convoluted by a Gaussian function representing the instrument response function (~180 fs, full width at half maximum; includes numeric broadening due to sampling ≥ 100 fs). Singular value decomposition [53] was applied to the data in order to ease the fitting procedure and to filter out noise. The fits were made simultaneously on the parallel and perpendicular data (not shown), sharing the same sum of exponentials. Effective fits of the isotropic or anisotropy data were deduced from them [32,34,39].

The fits are here presented using the so called evolution-associated difference spectra (EADS) [52], which correspond to a virtual cascading model with unity quantum yield between one state and the following and conveniently summarize the dynamics of the isotropic data. The anisotropy dynamics is similarly represented by evolution-associated anisotropy spectra (EAAS), deduced from the polarized EADS [32,34].

2.2.3. Spectral analysis

In order to analyze the spectral changes between consecutive EADS in terms of appearance and disappearance of certain photoproducts (namely the $TrpH^{\bullet+}$ and $Trp^{\bullet}$ radicals), we used an approach where the $EADS_{i+1} - (1\text{-}\phi_f)\ EADS_i$ difference is fitted by a sum of contributions from photoproducts. To improve the quality of the fits, the shape of reference spectra of the radicals [54] are slightly modified with the help of a shift and a scaling factor (see SI, Section S2.3). The details of that procedure have been

reported elsewhere [32,34]. Factor ϕ_r, which is optimally adjusted in the process, is the fraction of transient population at the start of phase i that undergoes ground state recovery (by charge recombination as will be seen below).

2.2.4. Anisotropy analysis

The anisotropy dynamics is essentially used here to monitor the origin of the $TrpH^{\bullet+}$ or $Trp^{\bullet}$ spectral signatures. Since several residues may contribute at this wavelength, the anisotropy can establish a difference between them based on their spatial orientation. As detailed in former works [32,34,39], the procedure first consists in choosing a proper monitoring wavelength at which the values of the EAAS, averaged over five nanometers, are taken (Table 2). For $TrpH^{\bullet+}$, we chose 600 nm, which lies on the red side of the $TrpH^{\bullet+}$ absorption band (see Figure S4 in SI, Section S2.3), in order to minimize the possible contribution of the reduced flavin radical ($FAD^{\bullet-}$) [55,56]. For $Trp^{\bullet}$, 530 nm was preferred, based on a similar argument. The experimental anisotropies are then compared to simulated ones (Table 3), expected at the monitoring wavelength if only one specific tryptophanyl species were contributing at a time. The simulated anisotropies are calculated [51] from the angle between the transition dipole moments of FAD_{ox} (73° from N_5N_{10} axis [39]) at the excitation wavelength and that of $TrpH^{\bullet+}$ (107.7° from $C_{3a}C_{7a}$ axis[39]) or $Trp^{\bullet}$ (104° from $C_{3a}C_{7a}$ axis [51]) at the monitoring wavelength. The orientations of the different species were taken from our homology model of *Ds*NewPHL (Figure 1) [40].

A tentative correction of the calculated anisotropies is proposed in Table 3 to take into account a possible minor contribution of $FAD^{\bullet-}$ at the monitoring wavelength. Following the example of former works [32,34], a maximum of 20% of the isotropic transient absorption at 600 nm is accepted to arise from $FAD^{\bullet-}$ once charge separation has occurred. This number rises to 25%, at 530 nm, when $TrpH^{\bullet+}$ is replaced by $Trp^{\bullet}$ (Figure S4). The procedure also requires a value of the intrinsic anisotropy of (pure) $FAD^{\bullet-}$ at the monitoring wavelength, which is here assumed to be the mean of two previously reported values (-0.2 [34] and -0.1 [32]), that is, -0.15. It should be noted that this approximate correction is merely intended to give an idea of the possible effect of $FAD^{\bullet-}$ contribution to the predictions.

2.3. Real-time TAS

The real-time transient absorption setup has been described in detail elsewhere [35,49,57]. Two different pulsed lasers were used as excitation sources: Continuum Leopard SS-10 Nd:YAG laser (~100 ps, 355 nm, ~5 $mJ.cm^{-2}$) and Nd:YAG-pumped optical parametric oscillator (OPO; Brilliant B/Rainbow; ~5 ns, 470 nm, ~2 $mJ.cm^{-2}$). The laser energy was estimated from energy measurements behind a cell filled with H_2O using an energy-meter (Gentec QE25SP-H-MB-D0) and from transient absorption signals using

$[Ru(bpy)_3]^{2+}$ as an actinometer [58]. Monitoring light at six selected wavelengths (376, 457, 488, 515, 562 and 690 nm) was provided by continuous-wave lasers and a laser diode (Toptica iBeam smart 375-S, Cobolt Twist™, Picarro Cyan-20, Cobolt Fandango™, Oxxius 561-25-COL-002 and Ondax TO-690-PLR45, respectively). The measuring light was perpendicular to the excitation laser beam and passed through the sample along the 10-mm path of a 2 × 2 × 10 mm (W × H × L) quartz cell with self-masking solid black walls (Starna). Flash-induced changes of the transmission of the sample were monitored behind the sample by a Si photodiode (Alphalas UPD-200-UP, 200 ps rise time) coupled to a digital oscilloscope (Agilent Infinium 81004B, 10 GHz, or Tektronics MSO 64, 200 MHz,). The samples were kept at 5 °C during the measurements and the stock on ice.

Real-time transient absorption kinetics were determined using Levenberg-Marquardt least-squares optimization algorithm in Origin 2020 (by OriginLab), fitting the trend lines according to the equation: $y(t) = A \times e^{-t/\tau} + y_0$ or $y(t) = A_1 \times e^{-t/\tau 1} + A_2 \times e^{-t/\tau 2} + y_0$ (global fits of all recorded signals).

3. RESULTS

3.1. Early photoinduced behavior of *Ds*NewPHL

3.1.1. Spectral evolution

Selected isotropic transient absorption spectra of *Ds*NewPHL in H_2O buffer, recorded between 200 fs and 3.2 ns after fs excitation at 470 nm, are shown in Figure 2(A-C). The shape of the earliest spectrum – with ground-state bleaching (GSB) at 444 nm, stimulated emission (SE) at 539 nm and transient absorption (TA) bands at 364 nm, 507 nm and beyond ~600 nm– are well characterized features of excited FAD_{ox} (here noted FAD*), often reported in other photolyases or cryptochromes [25,32,34,39,46], as well as free FAD_{ox} in solution [24,59].

The subsequent evolution, from 0.2 to 3.4 ps (Figure 2A), with decay of the SE and red TA bands and growth of a new positive band around 580 nm, have also been abundantly described [25,32,34,39,46]. It is assigned to the transfer of an electron from a Trp residue due to the FAD*, producing the $FAD^{\bullet-}/TrpH^{\bullet+}$ radical pair. $FAD^{\bullet-}$ still strongly absorbs in the UV TA region, at 367 nm, but shows a secondary peak at 400 nm [55,56,60], while $TrpH^{\bullet+}$ is responsible for the broad 580-nm band [54]. Virtually no decay of the GSB band can be seen during this primary ultrafast phase.

A second evolution phase, between 3.4 and ~400 ps (Figure 2B), sees a partial decay of the UV TA and GSB bands and an even more conspicuous decay of the 580-nm band, which nearly disappears, leaving a local maximum around 515 nm. The disappearance of the 580-nm band comes to completion during the last phase, between ~400 and 3200 ps (Figure 2C), during which one also observes a strong but still

partial decay of all bands. The last phase is also characterized by a modification of the shape of the UV TA band, which becomes rounder, somewhat red shifted and loses its secondary peak at 400 nm.

The transient absorption spectra of *Ds*NewPHL in a deuterated buffer are provided in Figure S2 (SI, Section S2.1). They are qualitatively identical to those in H_2O buffer, but the intermediate phase is significantly slower. One indeed observes that the remains of the 580-nm band at 388 ps pump-probe delay are significantly larger in D_2O than in H_2O.

3.1.2. Kinetic analysis

We could satisfactorily fit the parallel and perpendicular transient absorption spectra of *Ds*NewPHL with a sum of four exponential components followed by a plateau. Figure 3(A,C) displays the global fits corresponding to the measurements of Figure 2 (H_2O) and Figure S2 (D_2O), in terms of isotropic EADS (see Section 2.2.2). The same spectra, arbitrarily normalized at the maximum of the bleaching band (around 444 nm) are also proposed in Figure S3 (SI, Section S2.2), to better appreciate the changes of their shape. The evolution phases sketched above are here clearly quantified. The initial excited-state decay occurs with a time constant of 0.62 ps in H_2O buffer. The intermediate regime is decomposed in two time constants, 13 ps and 94 ps in H_2O. It may be noted that the 13 ps phase is mainly characterized by a substantial narrowing and structuring of the 580-nm band, as previously reported in similar timescales for other PCSf members [32,39]. The 94 ps phase carries most of the actual decay of the 580-nm band, mentioned above. The final kinetic phase occurs in 938 ps in H_2O.

Four independent measurements were actually made in H_2O buffer and two in D_2O, yielding very close results. Table 1 gathers the mean time constants obtained upon global fitting these recordings, namely 0.66, 13, 93 and 951 ps in H_2O and 0.67, 27, 146 and 1125 ps in D_2O. It appears then clearly that H/D exchange has no effect on the first time component (τ_1) but substantially slows down the following two components, by a factors of 2.1 (τ_2) and 1.6 (τ_3). A less significant kinetic isotope effect (factor of 1.2) remains on the final component (τ_4). As alluded above, it also clearly appears that EADS4 has a much larger intensity around 580 nm in D_2O buffer than in H_2O (see Discussion, Section 4.1.3).

3.1.3. Anisotropy dynamics

The raw transient anisotropy spectra, calculated from the polarized data are not shown but Figure 3 displays typical evolution-associated anisotropy spectra (EAAS) coming for the global analysis procedure. The initial phase is here accompanied by very large changes between 500 and 650 nm, essentially due to the decay of the negative SE band, substituted by a positive transient absorption band. The second phase is characterized by a clear change of anisotropy in the region around 580 nm where $TrpH^{\bullet+}$ mostly contributes. The value jumps from -0.08 in EAAS2 (mean value of four independent measurements in

H_2O buffer) to about +0.05 in EAAS3 (*idem*). During the third phase, the anisotropy beyond 550 nm becomes increasingly noisy due to the decay of the 580-nm isotropic band. The anisotropy of the remaining isotropic band around 515 nm however does not change much during the third phase. During the final kinetic phase, the anisotropy becomes unreliable above 550 nm because the corresponding isotropic spectra (denominator in the definition of *r*) nearly vanish.

3.2. Fate of the remaining transient absorption changes followed by real-time TAS

Real-time TAS signal recorded for *Ds*NewPHL (in H_2O) at 457 nm on a setup with ~200 ps time resolution (Figure S6 in SI, Section S3) captured the last (~950 ps) kinetic phase observed in the ultrafast experiment and the decay of most (>80 %) of the initial transient absorption signal. Note that the initial signal amplitude (at $t \rightarrow 0$) is slightly underestimated because the processes faster than 200 ps could not be resolved in this experiment.

Evolution of the remaining transient absorption change on the nanosecond timescale (*i.e.* beyond the red spectrum in Figure 2) was followed using a more sensitive real-time TAS setup with a time resolution limited to ~5 ns (excitation pulse duration). Transient absorption signals recorded at six selected monitoring wavelengths (Figure 5A) show that, following the ultrafast processes discussed above and reflected by the (not well resolved) initial sharp peaks in Figure 5A, the remaining TA signals decay almost entirely with common kinetics of ~50 ns. An exception is the signal at 690 nm, which is essentially zero from the very beginning and does not exhibit any significant evolution on this timescale. Comparison of the relative amplitudes of the sub-ns phase and the ~50 ns phase (Figure 5B) suggests that both processes reflect decays of spectrally identical species.

The small absorption change remaining after the ~50 ns phase has a spectrum (Figure S7B) compatible with the triplet state of FAD [61] and its lifetime (1.2 µs; Figure S8 in SI, Section 3) matches approximately that reported for the FAD triplet in solution (~3 µs [61]). Since its amplitude was seen to increase slightly when the sample was stored overnight at 0 °C, we assign it to a small population of free FAD released by the protein as it slowly degrades. This signal is therefore not considered as part to the photoinduced response of *Ds*NewPHL.

We finally note that a minute residual absorption change (< 0.5 mOD at 457 nm) may be observed after the decay of the FAD triplet state, lasting for tens of microseconds (Figure S8). Given the amplitude of the signal even close to the maximum of FAD bleaching was very small, we did not attempt a closer spectral characterization of this residual species but we do not exclude that it could constitute a minor long-lived decay channel belonging to the photoinduced response of *Ds*NewPHL.

4. DISCUSSION

4.1. Ultrafast photoreduction steps

4.1.1. Primary flavin reduction

As mentioned in Section 3.1, the transient absorption spectra show without ambiguity that the first phase in the photoreduction of oxidized *Ds*NewPHL *in vitro* is the transfer of an electron from a Trp residue to the excited flavin, with a time constant of 0.66 ps. This is quite a standard behavior in most oxidized PCSf members [17,24,25,32,39], although a much longer time constant (9 ps) has been reported for the same reaction type of a class II CPD photolyase, which depends on a totally different tryptophan triad for ET [34]. The charge separation yield of this phase is assumed to be 1 in *Ds*NewPHL on the basis of its extremely fast rate, efficiently preventing any ground-state recovery. This is in line with the virtual absence of decay of the GSB band, although this indicator is not fully reliable since the GSB band is highly overlapped with the transient absorption of the flavin, which evolves from FAD* to $FAD^{\bullet-}$.

The electron donor involved in phase 1 is most presumably the proximal Trp, which in the case of *Ds*NewPHL and according to our homology model (Figure 1) [40], is Trp_{192}. Trp_{192} is predicted to be located at an centroid-to-centroid distance of 5.5 Å (edge-to-edge 4.6 Å) from the isoalloxazine core of FAD and corresponds structurally to proximal tryptophans of other PCSf members apart the class II photolyases. Its assignment may be semi-quantitatively confirmed by examining the anisotropy at 600 nm, dominated by the $TrpH^{\bullet+}$ contribution, according to the procedure outlined in Section 2.2.4. The value of EAAS2, *i.e.* at the end of the 0.66 ps phase, at this wavelength is -0.08 (r_2, Table 2) while the simulated anisotropy for $Trp_{192}H^{\bullet+}$ is -0.03 (-0.05 with tentative $FAD^{\bullet-}$ correction; Table 3). Given the rather larger error on the prediction (see Table 3), it can be said that the experimental and theoretical values are essentially compatible. It may further be noted that the anisotropy attributed to the proximal $Trp_{192}H^{\bullet+}$ (r_2) is very similar to previously reported values (~ -0.06) for structurally analogous radicals (in canonical proximal position) in *Xenopus laevis* (6-4) photolyase [39] and *Chlamydomonas rheinhardtii* animal-like cryptochrome [32].

It may also be recalled that the isotropic EADS2 shows a quite broad spectral signature of $TrpH^{\bullet+}$, extending well over 650 nm (Figure 3 or Figure S3). Such a shape, which is significantly broader than that of $TrpH^{\bullet+}$ in solution [54], has previously been reported for other PCSf members [25,32,39] and been associated to the oxidized proximal Trp. The particular shape of EADS2 could be tentatively explained by

the fact that the $TrpH^{\bullet+}$ radical produced immediately after the initial ultrafast ET is in a hot vibrational state [25]. Alternatively, one might hypothesize that the proximal tryptophanyl radical would have a distinct absorption spectrum because of its close electrostatic interaction with the anionic flavin radical ($FAD^{\bullet-}$).

4.1.2. Hole transport

The second kinetic phase reported in Section 3.1.2, with a time constant of 13 ps, sees a clear narrowing of the $TrpH^{\bullet+}$ absorption signature around 580 nm upon the transition from EADS2 to EADS3 (see Figure 3 or Figure S3). Following the comment made above, this change might either be due to some vibrational cooling of the tryptophanyl radical or to a migration of the oxidation site away from the proximal Trp.

The anisotropy analysis provides here valuable information. One can indeed see in Table 2 that the value of EAAS3 at 600 nm (r_3) is 0.05 (in H_2O buffer; 0.09 in D_2O), which is closer this time to the simulated anisotropy of $Trp_{169}H^{\bullet+}$, namely 0.13 (0.08 with $FAD^{\bullet-}$ correction; Table 3). Within the prediction errors and the uncertain reliability of our homology model of *Ds*NewPHL, this can be taken as strong support to the hypothesis of electron hole migration, from $Trp_{192}H^{\bullet+}$ to Trp_{169}. It is interesting in this respect to observe that Trp_{169} is not the only close aromatic residue to Trp_{192}, as Trp_{161} has a centroid-to-centroid distance of 6.6 Å (edge-to-edge 3.7 Å) that is comparable to the 6.4 Å for Trp_{169} (Figure 1; edge-to-edge 4.2 Å). The simulated anisotropy of $Trp_{161}H^{\bullet+}$ is however much larger (0.30, 0.21 with $FAD^{\bullet-}$ correction; Table 3) and less compatible with the value of EAAS3 at 600 nm. Till a crystal structure of a NewPHL becomes available one may currently hypothesize that the migration of the positive charge preferentially goes in the direction of Trp_{169}. This preference might arise from the spatial arrangement of Trp_{192} and Trp_{169}, which are predicted to share the same kind of long "border" between the proximal and medial tryptophan (Figure 1) as other canonical PCSf members. The coplanar arrangement of their indole moieties potentially favors the overlap of donor-acceptor molecular orbitals and hence accelerates the ET rate. In contrast, the planes of the alternative pair Trp_{192} - Trp_{161} are essentially perpendicular in the NewPHL model. The polarity of the local environment of Trp_{169} might also be invoked, hypothetically, as a mean to favorably adjust the driving force and reorganization energy of the ET, as described within the Marcus theory [62,63]. Theoretical approaches have proven feasible to quantify such effects and calculate ET rates in several PCSf members [64-66] and other flavoproteins [67-69]. They might be applied to *Ds*NewPHL, once a crystal structure is resolved, to check this hypothesis further.

It should be noted from Figure 3 that phase 2 is accompanied by a moderate decay of the GSB and UV TA bands, interpreted as a partial charge recombination of the $FAD^{\bullet-}/Trp_{192}H^{\bullet+}$ pair, in competition with the migration of the positive charge. The recombination yield of this phase is evaluated to about 13% (of the transient population in EADS2) from the loss of GSB intensity.

Last but not least, one may recall that phase 2 demonstrates a clear H/D kinetic isotope effect (KIE) of 2.1. This is quite large and unexpected for a reaction that would merely involve forward, and possibly backward, ET steps. One possible explanation could be that some proton transfer is also involved during this kinetic phase, as will be seen for the following phase, although such a process does not clearly show up in the transient absorption spectra. One could alternatively propose that H/D exchange in the buffer has an indirect impact on the protein, *e.g.* by changing the strength of the H bonds [70], possibly due to water molecules entering deeply into the core of the protein and participating in its structure. Distances might thereby be altered, to which ET rates are known to be highly sensitive [63].

4.1.3. Tryptophanyl deprotonation

The third kinetic phase occurs in 93 ps and is characterized by a strong decay of the 580 nm band (Figure 3 and Figure S3), leaving a residual band around 515 nm and accompanied a further partial decay of the GSB and UV TA bands. Similar spectral evolutions have already been described for different oxidized PCSf members, in the context of tryptophanyl deprotonation after charge separation [20,34,35,37]. This process typically takes place in the hundred ns regime [5,20,37] in canonical PCSf members, but has been reported to occur in ~300 ps in a class II CPD photolyase [34,35].

We here confirmed the involvement of tryptophanyl deprotonation during phase 3 by using the spectral fitting approach sketched in Section 2.2.3. For that purpose, EADS4 was satisfactorily fitted with a sum of EADS3 and a difference of $TrpH^{\bullet+}$ and $Trp^{\bullet}$ absorption spectra taken from the literature and slightly modified to take into account spectral shifts and variations of width. The fit is shown in Figure 4, while the optimized parameters and modified radical spectra may be found in SI, Section S2.3. We find that the yield of charge recombination (ϕ_r) during phase 3 is ~15% of the transient population in EADS3 (13% of the transient population in EADS2) in H_2O buffer and ~13% in D_2O.

The yield of tryptophanyl deprotonation (ϕ_d) during phase 3 is not directly provided by the spectral fit because the $TrpH^{\bullet+}$ concentration at the start of the phase is not evaluated. This can however be estimated by analyzing the value of EADS3 in the red edge of the $TrpH^{\bullet+}$ band (at 600 nm), where the contribution of $FAD^{\bullet-}$ is minimal. The details of that calculation are provided in SI, Section S2.4. One finds that ϕ_d is ~79% of the transient population in EADS3 in H_2O and ~55% in D_2O. Interestingly, the lower

value of ϕ_d in D_2O, in line with a larger $TrpH^{\bullet+}$ signature in EADS4 (Figure 3C or Figure S3B), is not due to a larger charge recombination yield. It appears that $TrpH^{\bullet+}$ deprotonation is only partial in D_2O during phase 3, the completion of it taking place during phase 4 (see below), with final decay of the $TrpH^{\bullet+}$ band (better seen in Figure S3B). The meaning of this result is not clear to us but we imagine that, if solvation in the D_2O buffer leads to small structural changes with respect to the structure in the H_2O buffer, Trp_{161} could participate in ET to a larger extent in D_2O –note that the value of r_5 is rather different in H_2O (0.08) and D_2O (0.21) and that r_5 in D_2O fits the corrected simulated anisotropy of $Trp_{161}^{\bullet}$ (0.19) better than that of $Trp_{169}^{\bullet}$ (0.09).

The discussion of Section 4.1.2 suggests that the tryptophanyl undergoing deprotonation during kinetic phase 3 is essentially $Trp_{169}H^{\bullet+}$. This assignment is supported by the anisotropy observed in EAAS4 (r_4, Table 2) at 530 nm, where the contribution of $Trp^{\bullet}$ is dominant (see Figure S4). One finds 0.12 (in H_2O buffer; 0.09 in D_2O), which is not far within errors from the simulated anisotropy of $Trp_{169}^{\bullet}$ (between 0.17 and 0.09, Table 3). The possible contribution of $Trp_{161}^{\bullet}$ is thus at this stage not favored in the H_2O buffer.

The nature of the primary proton acceptor involved in this kinetic phase is at the moment not identified. We may however conceive that a cluster of protein-bound water molecules could potentially play this role, as was previously reported for the class II CPD photolyase mentioned above [35], as its tryptophanyl deprotonation is also unusually fast. However, this hypothesis requires confrontation with a high-resolution crystal structure of a NewPHL protein.

4.1.4. Charge recombination and stabilization

We have seen in previous sections that charge recombination of the $FAD^{\bullet-}/TrpH^{\bullet+}$ pair occurs during the second and third kinetic phases (13 and 93 ps in H_2O buffer), with successive yields of about 13% and 15%, respectively. A much larger degree of charge recombination is observed during the fourth phase (951 ps). Using the decay of the GSB maximum between EADS4 and EADS5, one calculates a yield of charge recombination of 86% of the transient population in EADS4 (64% of the transient population in EADS2) for that phase alone. Overall, the successive recombination steps represent 13%, 13% and 64% of the initial charge separated population (in EADS2). Including all three steps, the total yield of charge recombination amounts to 90%. As previously commented for other photolyases [17,34,39], it is likely that fast charge recombination during the sub-ns phases actually takes place from the proximal $FAD^{\bullet-}/TrpH^{\bullet+}$ pair (because the radicals are here separated by a shorter, more favorable distance) that would be weakly repopulated by some back electron/proton transfers –presently unresolved.

The fourth kinetic phase (~950 ps) is characterized by a marked modification of the UV transient absorption band, which develops a maximum at 380 nm in EADS5, while EADS4 peaks at 367 nm (better seen in Figure S3). The red shoulder of this band also seems to be significantly altered as one observes that the maximum of the GSB band shifts from 444 to 436 nm. The exact origin of these spectral changes is not clear to us but one may hypothesize that they arise from changes in the hydrogen-bonding network around the flavin. For instance, a similar spectral change (narrowing down, shift and diminishing of the $FAD^{\bullet-}$ UV band and shift of the shoulder in the visible) was reported for the N378D mutant of *Ec*CPD upon photoreduction of an artificially fully oxidized FAD cofactor [20]. The authors suggested that unlike in most other photolyases and cryptochromes, $FAD^{\bullet-}$ does not get protonated in this particular case (or only to a very small extent) and is stabilized by mere hydrogen bonding to the neighboring amino acid instead. In the case of *Ds*NewPHL, one can imagine that $FAD^{\bullet-}$ could be stabilized by forming an H-bond, *e.g.* to the amide group of N_{188} side chain. It may be further supposed that such structural changes would help stabilizing the $FAD^{\bullet-}/Trp^{\bullet}$ pair radical, possibly by slowing down some back ET channels involved in charge recombination.

4.2. Final charge recombination step

Global bi-exponential fit of all data, shown in Figure S7A, yielded time constants of ~2 ns and ~50 ns. The ~2 ns phase actually corresponds to the ~950 ps phase reported above, which was not well resolved by the real-time TAS setup used here. Plotting the amplitudes of the individual phases against wavelength and comparing them with the combined spectra of FAD and Trp radical species from the literature suggest that both processes reflect the recombination of $FAD^{\bullet-}/Trp^{\bullet}$ radical pairs (Figure 5B and S7B). It is however unclear, whether the biphasic characteristics of this process is due to recombination of $FAD^{\bullet-}$ with a heterogeneous mixture of two different $Trp^{\bullet}$ species (*e.g.* majority of $Trp_{169}^{\bullet}$ and minority of $Trp_{161}^{\bullet}$) or due to a stabilization of one or both radicals in the $FAD^{\bullet-}/Trp_{169}^{\bullet}$ pair during the ~950 ps phase. Study of mutants of Trp_{169} and Trp_{161}, which is beyond the scope of the current paper, should provide an answer to this question. Theoretical approaches such as the ones alluded to above [64-69] might also provide clarifications on the precise mechanisms of charge recombination at work in *Ds*NewPHL.

It is then interesting to establish a relation between the photoinduced response of oxidized *Ds*NewPHL observed here and its reported photoreduction *in vitro* [40]. The fastest decay component with which reduction by the external electron donor (50 mM DTT) could possibly compete is the ~50 ns phase. For the sake of comparison, let us recall that the terminal radical recombination in other WT

photolyases typically occurs on the ms timescale [18,20,37,58], which leaves considerably more time for external reduction. The case of the W370F mutant of the (6-4) photolyase from *Xenopus laevis* (*Xl*64) is closer to *Ds*NewPHL because its final charge recombination takes place in only 10 µs [37], and its photoreduction is possible *in vitro* (with 6 mM cysteine) [44] –yet highly impaired as compared to the WT protein. We however highlight that the decay of the $FAD^{\bullet-}/Trp^{\bullet}$ radical pair in *Xl*64-W370F is still 200 times slower than that in *Ds*NewPHL and hence much more favorable to competition by external reduction. The decay of *Ec*CPD-W306F (~1 µs, in semi-reduced form [42]) is only 20 times slower and, in that case, *in vitro* photoreduction was reported to be absent [41]. We therefore anticipate that external reduction in competition with the ~50 ns phase of *Ds*NewPHL should be extremely inefficient, even at a DTT concentration of 50 mM. We rather suggest that *in vitro* photoreduction proceeds in competition with the very weak, longer-lived component that we could detect as residual FAD_{ox} bleaching at 457 and 488 nm on the µs timescale (Figure S8 and Section 3.2).

The efficiency of such a photoreduction channel is however doubtful *in vivo*, as the cytosolic reductant concentrations, diffusion conditions and intensity of available light (not absorbed by other present chromophores) are likely much less favorable than in the *in vitro* experiment [40]. The case of the (6-4) photolyase from *Xenopus laevis* (*Xl*64) illustrates this situation quite well: even though *Xl*64-W370F is still photoreducible and active for DNA repair *in vitro*, it has been found inactive for DNA repair in *E. coli* [44]. This was interpreted by the impairment of photoreduction *in vivo*, due to fast radical pair recombination (10 µs) of this mutant –4000 times faster than the WT [37].

5. CONCLUSIONS

We have shown that the photoreduction dynamics of oxidized *Ds*NewPHL begins similarly as that of canonical photolyases or cryptochromes, with a sub-ps primary reduction of the excited flavin by the adjacent Trp (0.7 ps phase), followed by migration of the electron hole towards the second Trp in the tens of ps regime (13 ps phase), in competition with modest charge recombination. We then observed a very fast deprotonation of the $TrpH^{\bullet+}$ radical, with a time constant of ~90 ps. This is more than three orders of magnitude faster than in any other canonical PCSf member [5,20,37] and still about three times faster than in the recently reported case of a non-canonical class II CPD photolyase [34,35]. In spite of this unprecedentedly fast deprotonation, which helps stabilizing charge separation [43], charge recombination massively takes place in a subsequent ~950 ps phase. Globally, ~90% of all photoinduced

radical pairs are lost within a few nanoseconds and the remaining ~10% is seen to almost fully disappear in less than 200 ns (~50 ns phase). A very weak signal however remains on the µs timescale, which could not be spectrally identified. Figure 6 summarizes the whole dynamics (the long-lived residual is not represented in this scheme because it is very weak and has insufficiently been resolved). Such a rapid and almost complete recombination of the radical pairs in the ns timescale leaves virtually no time for extrinsic reductants to act upon the Trp radicals, or for extrinsic proton donors to stabilize $FAD^{\bullet-}$ *in vivo*, although the weak long-lived time decay component could explain the possibility of photoreduction *in vitro* [40]. We therefore conclude that the first photoreduction step, that is, conversion of fully oxidized FAD to the semi-quinone form $FADH^{\bullet}$, should be essentially impossible in *Ds*NewPHL *in vivo*.

While this step is the basis of signaling by cryptochromes and the initial step in photoactivation of some photolyases [37,44,57], we believe that it is unlikely to play any significant role in *Ds*NewPHL. This situation could be understood within the picture established for *Ec*CPD by Payne *et al.* [71], namely that photoreduction is *per se* not required *in vivo*, *i.e.* in *E. coli*, because the flavin is already fully reduced in the dark. It could similarly be that the oxidation state of the flavin in *Ds*NewPHL in the dark, within *Dinoroseobacter shibae*, would be either fully or semi-reduced. Notably, recombinant *Ds*NewPHL contains $FADH^{\bullet}$ when purified under aerobic conditions and the $FADH^{-}$ state when isolated under anaerobic conditions [40]. If that is the case in *Dinoroseobacter shibae*, the biologically relevant step leading to photoactivation of DNA repair [40] will be the second photoreduction step, from $FADH^{\bullet}$ to $FADH^{-}$. Spectroscopic characterization of the dynamics of this process will be subject of our future investigations.

CONFLICT OF INTERESTS

There are no conflicts to declare.

ACKNOWLEDGEMENTS

The present work has benefited from the platform of Biophysics of I2BC supported by French Infrastructure for Integrated Structural Biology (FRISBI) ANR-10-INBS-05.

REFERENCES

1. Sancar, A. (2003). Structure and function of DNA photolyase and cryptochrome blue-light photoreceptors. *Chemical Reviews, 103*(6), 2203-2237, https://doi.org/10.1021/cr0204348.
2. Cadet, J., Sage, E., & Douki, T. (2005). Ultraviolet radiation-mediated damage to cellular DNA. *Mutation Research, 571*(1-2), 3-17, https://doi.org/10.1016/j.mrfmmm.2004.09.012.

3. Weber, S. (2005). Light-driven enzymatic catalysis of DNA repair: a review of recent biophysical studies on photolyase. *Biochimica et Biophysica Acta - Bioenergetics, 1707*(1), 1-23, https://doi.org/10.1016/j.bbabio.2004.02.010.
4. Müller, M., & Carell, T. (2009). Structural biology of DNA photolyases and cryptochromes. *Current Opinion in Structural Biology, 19*(3), 277-285, https://doi.org/10.1016/j.sbi.2009.05.003.
5. Brettel, K., & Byrdin, M. (2010). Reaction mechanisms of DNA photolyase. *Current Opinion in Structural Biology, 20*, 693-701, https://doi.org/10.1016/j.sbi.2010.07.003.
6. Yamamoto, J., Plaza, P., & Brettel, K. (2017). Repair of (6-4) lesions in DNA by (6-4) photolyase: 20 years of quest for the photoreaction mechanism. *Photochemistry and Photobiology, 93*(1), 51-66, https://doi.org/10.1111/php.12696.
7. Ritz, T., Adem, S., & Schulten, K. (2000). A model for photoreceptor-based magnetoreception in birds. *Biophysical Journal, 78*(2), 707-718, https://doi.org/10.1016/s0006-3495(00)76629-x.
8. Cashmore, A. R. (2003). Cryptochromes: enabling plants and animals to determine circadian time. *Cell, 114*(5), 537-543, https://doi.org/10.1016/j.cell.2003.08.004.
9. Chaves, I., Pokorny, R., Byrdin, M., Hoang, N., Ritz, T., Brettel, K., Essen, L.-O., van der Horst, G. T. J., Batschauer, A., & Ahmad, M. (2011). The cryptochromes: blue light photoreceptors in plants and animals. *Annual Review of Plant Biology, 62*, 335-364, https://doi.org/10.1146/annurev-arplant-042110-103759.
10. Hore, P. J., & Mouritsen, H. (2016). The radical-pair mechanism of magnetoreception. *Annual Review of Biophysics, 45*, 299-344, https://doi.org/10.1146/annurev-biophys-032116-094545.
11. Wang, Q., & Lin, C. (2020). Mechanisms of cryptochrome-mediated photoresponses in plants. *Annual Review of Plant Biology, 71*, 103-129, https://doi.org/10.1146/annurev-arplant-050718-100300.
12. Heelis, P. F., & Sancar, A. (1986). Photochemical properties of *Escherichia coli* DNA photolyase: a flash photolysis study. *Biochemistry, 25*(25), 8163-8166, https://doi.org/10.1021/bi00373a006.
13. Okamura, T., Sancar, A., Heelis, P. F., Hirata, Y., & Mataga, N. (1989). Doublet-quartet intersystem crossing of flavin radical in DNA photolyase. *Journal of the American Chemical Society, 111*(15), 5967-5969, https://doi.org/10.1021/ja00197a082.
14. Heelis, P. F., Okamura, T., & Sancar, A. (1990). Excited-state properties of *Escherichia coli* DNA photolyase in the picosecond to millisecond time scale. *Biochemistry, 29*(24), 5694-5698, https://doi.org/10.1021/bi00476a008.
15. Aubert, C., Vos, M. H., Mathis, P., Eker, A. P. M., & Brettel, K. (2000). Intraprotein radical transfer during photoactivation of DNA photolyase. *Nature, 405*(6786), 586-590, https://doi.org/10.1038/35014644
16. Lukacs, A., Eker, A. P. M., Byrdin, M., Brettel, K., & Vos, M. H. (2008). Electron hopping through the 15 Angström triple tryptophan molecular wire in DNA photolyase occurs within 30 ps. *Journal of the American Chemical Society, 130*(44), 14394-14395, https://doi.org/10.1021/ja805261m.
17. Liu, Z. Y., Tan, C., Guo, X. M., Li, J., Wang, L. J., Sancar, A., & Zhong, D. P. (2013). Determining complete electron flow in the cofactor photoreduction of oxidized photolyase. *Proceedings of the National Academy of Sciences of the United States of America, 110*(32), 12966-12971, https://doi.org/10.1073/pnas.1311073110.
18. Byrdin, M., Lukacs, A., Thiagarajan, V., Eker, A. P. M., Brettel, K., & Vos, M. H. (2010). Quantum yield measurements of short-lived photoactivation intermediates in DNA photolyase: toward a detailed understanding of the triple tryptophan electron transfer chain. *The Journal of Physical Chemistry A, 114*(9), 3207-3214, https://doi.org/10.1021/jp9093589.
19. Liu, Z. Y., Tan, C., Guo, X. M., Li, J., Wang, L. J., & Zhong, D. P. (2014). Dynamic determination of active-site reactivity in semiquinone photolyase by the cofactor photoreduction. *Journal of Physical Chemistry Letters, 5*(5), 820-825, https://doi.org/10.1021/jz500077s.

20. Müller, P., Brettel, K., Grama, L., Nyitrai, M., & Lukacs, A. (2016). Photochemistry of wild-type and N378D mutant *E. coli* DNA photolyase with oxidized FAD cofactor studied by transient absorption spectroscopy. *ChemPhysChem, 17*(9), 1329-1340, https://doi.org/10.1002/cphc.201501077.
21. Engelhard, C., Wang, X., Robles, D., Moldt, J., Essen, L.-O., Batschauer, A., Bittl, R., & Ahmad, M. (2014). Cellular metabolites enhance the light sensitivity of *Arabidopsis* cryptochrome through alternate electron transfer pathways. *Plant Cell, 26*(11), 4519-4531, https://doi.org/10.1105/tpc.114.129809.
22. Ignatz, E., Geisselbrecht, Y., Kiontke, S., & Essen, L. O. (2018). Nicotinamide adenine dinucleotides arrest photoreduction of class II DNA photolyases in $FADH^{\bullet}$ state. *Photochemistry and Photobiology, 94*(1), 81-87, https://doi.org/10.1111/php.12834.
23. Kao, Y. T., Tan, C., Song, S. H., Ozturk, N., Li, J., Wang, L. J., Sancar, A., & Zhong, D. P. (2008). Ultrafast dynamics and anionic active states of the flavin cofactor in cryptochrome and photolyase. *Journal of the American Chemical Society, 130*(24), 7695-7701, https://doi.org/10.1021/ja801152h.
24. Brazard, J., Usman, A., Lacombat, F., Ley, C., Martin, M. M., & Plaza, P. (2011). New insights into the ultrafast photophysics of oxidized and reduced FAD in solution. *The Journal of Physical Chemistry A, 115*(15), 3251-3262, https://doi.org/10.1021/jp110741y.
25. Immeln, D., Weigel, A., Kottke, T., & Perez Lustres, J. L. (2012). Primary events in the blue light sensor plant cryptochrome: intraprotein electron and proton transfer revealed by femtosecond spectroscopy. *Journal of the American Chemical Society, 134*(30), 12536-12546, https://doi.org/10.1021/ja302121z.
26. Biskup, T., Hitomi, K., Getzoff, E. D., Krapf, S., Koslowski, T., Schleicher, E., & Weber, S. (2011). Unexpected electron transfer in cryptochrome identified by time-resolved EPR spectroscopy. *Angewandte Chemie-International Edition, 50*(52), 12647-12651, https://doi.org/10.1002/anie.201104321.
27. Krapf, S., Weber, S., & Koslowski, T. (2012). The road not taken: a theoretical view of an unexpected cryptochrome charge transfer path. *Physical Chemistry Chemical Physics, 14*(32), 11518-11524, https://doi.org/10.1039/c2cp40793k.
28. Aubert, C., Mathis, P., Eker, A. P. M., & Brettel, K. (1999). Intraprotein electron transfer between tyrosine and tryptophan in DNA photolyase from *Anacystis nidulans*. *Proceedings of the National Academy of Sciences of the United States of America, 96*, 5423-5427, https://doi.org/10.1073/pnas.96.10.5423.
29. Giovani, B., Byrdin, M., Ahmad, M., & Brettel, K. (2003). Light-induced electron transfer in a cryptochrome blue-light photoreceptor. *Nature Structural Biology, 10*(6), 489-490, https://doi.org/10.1038/nsb933.
30. Biskup, T., Paulus, B., Okafuji, A., Hitomi, K., Getzoff, E. D., Weber, S., & Schleicher, E. (2013). Variable electron transfer pathways in an amphibian cryptochrome. *Journal of Biological Chemistry, 288*(13), 9249-9260, https://doi.org/10.1074/jbc.M112.417725.
31. Geisselbrecht, Y., Fruehwirth, S., Schroeder, C., Pierik, A. J., Klug, G., & Essen, L.-O. (2012). CryB from *Rhodobacter sphaeroides*: a unique class of cryptochromes with new cofactors. *EMBO Reports, 13*(3), 223-229, https://doi.org/10.1038/embor.2012.2.
32. Lacombat, F., Espagne, A., Dozova, N., Plaza, P., Müller, P., Brettel, K., Franz-Badur, S., & Essen, L.-O. (2019). Ultrafast oxidation of a tyrosine by proton-coupled electron transfer promotes light activation of an animal-like cryptochrome. *Journal of the American Chemical Society, 141*(34), 13394–13409, https://doi.org/10.1021/jacs.9b03680.
33. Kiontke, S., Geisselbrecht, Y., Pokorny, R., Carell, T., Batschauer, A., & Essen, L.-O. (2011). Crystal structures of an archaeal class II DNA photolyase and its complex with UV-damaged duplex DNA. *EMBO Journal, 30*(21), 4437-4449, https://doi.org/10.1038/emboj.2011.313.

34. Lacombat, F., Espagne, A., Dozova, N., Plaza, P., Ignatz, E., Kiontke, S., & Essen, L.-O. (2018). Femtosecond transient absorption study of the primary photoreduction events of a class II photolyase. *Physical Chemistry Chemical Physics, 20*, 25446-25457, https://doi.org/10.1039/C8CP04548H
35. Müller, P., Ignatz, E., Kiontke, S., Brettel, K., & Essen, L. O. (2018). Sub-nanosecond tryptophan radical deprotonation mediated by a protein-bound water cluster in class II DNA photolyases. *Chemical Science, 9*(5), 1200-1212, https://doi.org/10.1039/c7sc03969g.
36. Scheerer, P., Zhang, F., Kalms, J., von Stetten, D., Krauß, N., Oberpichler, I., & Lamparter, T. (2015). The class III cyclobutane pyrimidine dimer photolyase structure reveals a new antenna chromophore binding site and alternative photoreduction pathways. *Journal of Biological Chemistry, 290*(18), 11504-11514, https://doi.org/10.1074/jbc.M115.637868.
37. Müller, P., Yamamoto, J., Martin, R., Iwai, S., & Brettel, K. (2015). Discovery and functional analysis of a 4th electron-transferring tryptophan conserved exclusively in animal cryptochromes and (6-4) photolyases. *Chemical Communications, 51*, 15502-15505, https://doi.org/10.1039/c5cc06276d.
38. Nohr, D., Franz, S., Rodriguez, R., Paulus, B., Essen, L. O., Weber, S., & Schleicher, E. (2016). Extended electron-transfer in animal cryptochromes mediated by a tetrad of aromatic amino acids. *Biophysical Journal, 111*(2), 301-311, https://doi.org/10.1016/j.bpj.2016.06.009.
39. Martin, R., Lacombat, F., Espagne, A., Dozova, N., Plaza, P., Yamamoto, J., Müller, P., Brettel, K., & de la Lande, A. (2017). Ultrafast flavin photoreduction in an oxidized animal (6-4) photolyase through an unconventional tryptophan tetrad. *Physical Chemistry Chemical Physics, 19*(36), 24493-24504, https://doi.org/10.1039/c7cp04555g.
40. Emmerich, H. J., Saft, M., Schneider, L., Kock, D., Batschauer, A., & Essen, L. O. (2020). A topologically distinct class of photolyases specific for UV lesions within single-stranded DNA. *Nucleic Acids Research, 48*(22), 12845-12857, https://doi.org/10.1093/nar/gkaa1147.
41. Li, Y. F., Heelis, P. F., & Sancar, A. (1991). Active site of DNA photolyase: tryptophan-306 is the intrinsic hydrogen atom donor essential for flavin radical photoreduction and DNA repair i*n vitro*. *Biochemistry, 30*(25), 6322-6329, https://doi.org/10.1021/bi00239a034.
42. Byrdin, M., Villette, S., Eker, A. P. M., & Brettel, K. (2007). Observation of an intermediate tryptophanyl radical in W306F mutant DNA photolyase from *Escherichia coli* supports electron hopping along the triple tryptophan chain. *Biochemistry, 46*(35), 10072-10077, https://doi.org/10.1021/bi700891f.
43. Byrdin, M., Sartor, V., Eker, A. P. M., Vos, M. H., Aubert, C., Brettel, K., & Mathis, P. (2004). Intraprotein electron transfer and proton dynamics during photoactivation of DNA photolyase from *E. coli*: review and new insights from an "inverse" deuterium isotope effect. *Biochimica et Biophysica Acta - Bioenergetics, 1655*(1-3), 64-70, https://doi.org/10.1016/j.bbabio.2003.07.001.
44. Yamamoto, J., Shimizu, K., Kanda, T., Hosokawa, Y., Iwai, S., Plaza, P., & Muller, P. (2017). Loss of fourth electron-transferring tryptophan in animal (6-4) photolyase impairs DNA repair activity in bacterial cells. *Biochemistry, 56*(40), 5356-5364, https://doi.org/10.1021/acs.biochem.7b00366.
45. Macheroux, P. (1999). UV-visible spectroscopy as a tool to study flavoproteins. In S. K. Chapman, & G. A. Reid (Eds.), *Flavoprotein Protocols* (pp. 1-7, Methods in Molecular Biology, Vol. 131).
46. Brazard, J., Usman, A., Lacombat, F., Ley, C., Martin, M. M., Plaza, P., Mony, L., Heijde, M., Zabulon, G., & Bowler, C. (2010). Spectro-temporal characterization of the photoactivation mechanism of two new oxidized cryptochrome/photolyase photoreceptors. *Journal of the American Chemical Society, 132*(13), 4935-4945, https://doi.org/10.1021/ja1002372.
47. Yadav, D., Lacombat, F., Dozova, N., Rappaport, F., Plaza, P., & Espagne, A. (2014). Real-time monitoring of chromophore isomerization and deprotonation during the photoactivation of the fluorescent protein Dronpa. *The Journal of Physical Chemistry B, 119*(6), 2404-2414, https://doi.org/10.1021/jp507094f.

48. Yoshimura, A., Hoffman, M. Z., & Sun, H. (1993). An evaluation of the excited-state absorption-spectrum of $Ru(bpy)_3^{2+}$ in aqueous and acetonitrile solutions. *Journal of Photochemistry and Photobiology A: Chemistry, 70*(1), 29-33, https://doi.org/10.1016/1010-6030(93)80005-t.
49. Byrdin, M., Thiagarajan, V., Villette, S., Espagne, A., & Brettel, K. (2009). Use of ruthenium dyes for subnanosecond detector fidelity testing in real time transient absorption. *Review of Scientific Instruments, 80*(4), 043102, https://doi.org/10.1063/1.3117208.
50. Ekvall, K., van der Meulen, P., Dhollande, C., Berg, L. E., Pommeret, S., Naskrecki, R., & Mialocq, J. C. (2000). Cross phase modulation artifact in liquid phase transient absorption spectroscopy. *Journal of Applied Physics, 87*(5), 2340-2352, https://doi.org/10.1063/1.372185.
51. Byrdin, M., Villette, S., Espagne, A., Eker, A. P. M., & Brettel, K. (2008). Polarized transient absorption to resolve electron transfer between tryptophans in DNA photolyase. *The Journal of Physical Chemistry B, 112*(22), 6866-6871, https://doi.org/10.1021/jp711435y.
52. van Stokkum, I. H. M., Delmar, S. L., & van Grondelle, R. (2004). Global and target analysis of time-resolved spectra. *Biochimica et Biophysica Acta - Bioenergetics, 1657*(2-3), 82-104, https://doi.org/10.1016/j.bbabio.2004.04.011.
53. Henry, E. R., & Hofrichter, J. (1992). Singular value decomposition - Application to analysis of experimental data. *Methods in Enzymology, 210*, 129-193, https://doi.org/10.1016/0076-6879(92)10010-B.
54. Solar, S., Getoff, N., Surdhar, P. S., Armstrong, D. A., & Singh, A. (1991). Oxidation of tryptophan and N-methylindole by $N_3^{\bullet}$, $Br_2^{\bullet-}$, and $(SCN)_2^{\bullet-}$ radicals in light-water and heavy-water solutions: a pulse radiolysis study. *The Journal of Physical Chemistry, 95*(9), 3639-3643, https://doi.org/10.1021/j100162a038.
55. Berndt, A., Kottke, T., Breitkreuz, H., Dvorsky, R., Hennig, S., Alexander, M., & Wolf, E. (2007). A novel photoreaction mechanism for the circadian blue light photoreceptor *Drosophila* cryptochrome. *Journal of Biological Chemistry, 282*(17), 13011-13021, https://doi.org/10.1074/jbc.M608872200.
56. Liu, B., Liu, H., Zhong, D., & Lin, C. (2010). Searching for a photocycle of the cryptochrome photoreceptors. *Current Opinion in Plant Biology, 13*(5), 578-586, https://doi.org/10.1016/j.pbi.2010.09.005.
57. Müller, P., Bouly, J.-P., Hitomi, K., Balland, V., Getzoff, E. D., Ritz, T., & Brettel, K. (2014). ATP binding turns plant cryptochrome into an efficient natural photoswitch. *Scientific Reports, 4*, 5175, https://doi.org/10.1038/srep05175.
58. Müller, P., & Brettel, K. (2012). $[Ru(bpy)_3]^{2+}$ as a reference in transient absorption spectroscopy: differential absorption coefficients for formation of the long-lived 3MLCT excited state. *Photochemical & Photobiological Sciences, 11*(4), 632-636, https://doi.org/10.1039/c2pp05333k.
59. Weigel, A., Dobryakov, A., Klaumünzer, B., Sajadi, M., Saalfrank, P., & Ernsting, N. P. (2011). Femtosecond stimulated Raman spectroscopy of flavin after optical excitation. *The Journal of Physical Chemistry B, 115*(13), 3656-3680, https://doi.org/10.1021/jp1117129.
60. Massey, V., & Palmer, G. (1966). On existence of spectrally distinct classes of flavoprotein semiquinones . A new method for quantitative production of flavoprotein semiquinones. *Biochemistry, 5*(10), 3181-3189, https://doi.org/10.1021/bi00874a016.
61. Gauden, M., Yeremenko, S., Laan, W., van Stokkum, I. H. M., Ihalainen, J. A., van Grondelle, R., Hellingwerf, K. J., & Kennis, J. T. M. (2005). Photocycle of the flavin-binding photoreceptor AppA, a bacterial transcriptional antirepressor of photosynthesis genes. *Biochemistry, 44*(10), 3653-3662, https://doi.org/10.1021/bi047359a.
62. Marcus, R. A., & Sutin, N. (1985). Electron transfers in chemistry and biology. *Biochimica et Biophysica Acta, 811*, 265-322, https://doi.org/10.1016/0304-4173(85)90014-X.

63. Moser, C. C., & Dutton, P. L. (1992). Engineering protein-structure for electron-transfer function in photosynthetic reaction centers. *Biochimica et Biophysica Acta, 1101*(2), 171-176, https://doi.org/10.1016/0005-2728(92)90205-g.
64. Popović, D. M., Zmirić, A., Zarić, S. D., & Knapp, E.-W. (2002). Energetics of Radical Transfer in DNA Photolyase. *Journal of the American Chemical Society, 124*(14), 3775-3782, https://doi.org/10.1021/ja016249d.
65. Lüdemann, G., Solov'yov, I. A., Kubař, T., & Elstner, M. (2015). Solvent Driving Force Ensures Fast Formation of a Persistent and Well-Separated Radical Pair in Plant Cryptochrome. *Journal of the American Chemical Society, 137*(3), 1147-1156, https://doi.org/10.1021/ja510550g.
66. Cailliez, F., Muller, P., Firmino, T., Pernot, P., & de la Lande, A. (2016). Energetics of Photoinduced Charge Migration within the Tryptophan Tetrad of an Animal (6-4) Photolyase. *Journal of the American Chemical Society, 138*(6), 1904-1915, https://doi.org/10.1021/jacs.5b10938.
67. Nunthaboot, N., Tanaka, F., Kokpol, S., Chosrowjan, H., Taniguchi, S., & Mataga, N. (2009). Simulation of ultrafast non-exponential fluorescence decay induced by electron transfer in FMN binding protein. *Journal of Photochemistry and Photobiology A: Chemistry, 201*(2-3), 191-196, https://doi.org/10.1016/j.jphotochem.2008.10.025.
68. Tanaka, F., Lugsanangarm, K., Nunthaboot, N., Nueangaudom, A., Pianwanit, S., Kokpol, S., Taniguchi, S., & Chosrowjan, H. (2015). Classification of the mechanisms of photoinduced electron transfer from aromatic amino acids to the excited flavins in flavoproteins. *Physical Chemistry Chemical Physics, 17*(26), 16813-16825, https://doi.org/10.1039/c5cp01432h.
69. Lugsanangarm, K., Tamaoki, H., Nishina, Y., Kitamura, M., Nunthaboot, N., Tanaka, F., Taniguchi, S., & Chosrowjan, H. (2020). Simultaneous analyses of the rates of photoinduced charge separation and recombination between the excited flavin and tryptophans in some flavoproteins: Molecular dynamics simulation. *AIP Advances, 10*(10), 14, https://doi.org/10.1063/5.0014718.
70. Scheiner, S., & Čuma, M. (1996). Relative stability of hydrogen and deuterium bonds. *Journal of the American Chemical Society, 118*(6), 1511-1521, https://doi.org/10.1021/ja9530376.
71. Payne, G., Heelis, P. F., Rohrs, B. R., & Sancar, A. (1987). The active form of *Escherichia coli* DNA photolyase contains a fully reduced flavin and not a flavin radical, both i*n vivo* and *in vitro*. *Biochemistry, 26*(22), 7121-7127, https://doi.org/10.1021/bi00396a038.

FIGURES

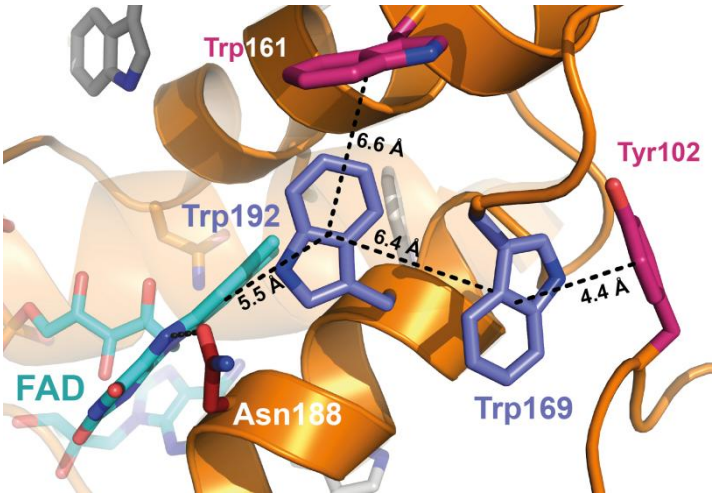

Figure 1. View of the *Ds*NewPHL structure at the flavin binding site, as derived from a homology model of the protein [40], taking the *Anacystis nidulans* class I CPD photolyase (PDB entry 1TEZ) as a template. FAD is represented in cyan, the conserved tryptophan dyad (Trp_{192}, Trp_{169}) of NewPHL in blue and the nearby residues Tyr_{102} and another tryptophan (Trp_{161}) in pink. Closest centroid-centroid distances between the aromatic moieties are indicated. Asn_{188} (red) is predicted to form a hydrogen-bond with the N_5-nitrogen of the isoalloxazine moiety,

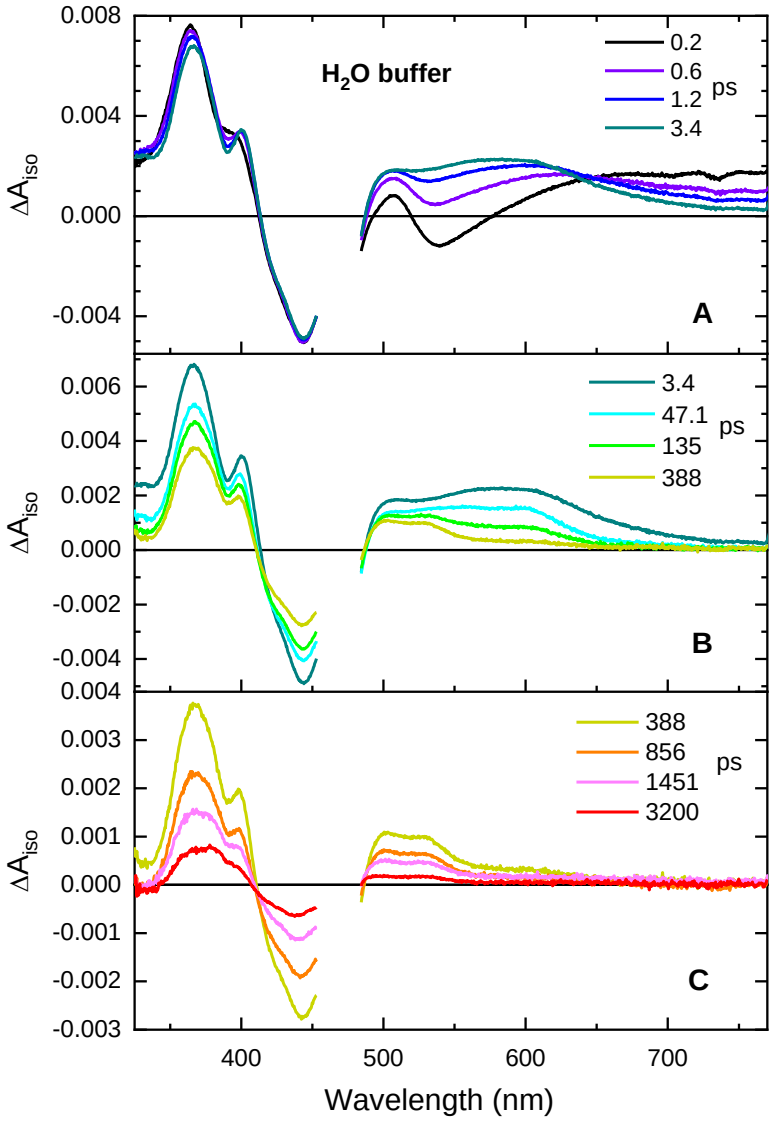

Figure 2. Isotropic transient absorption spectra of *Ds*NewPHL in H_2O buffer, at selected pump-probe delays after fs excitation at 470 nm.

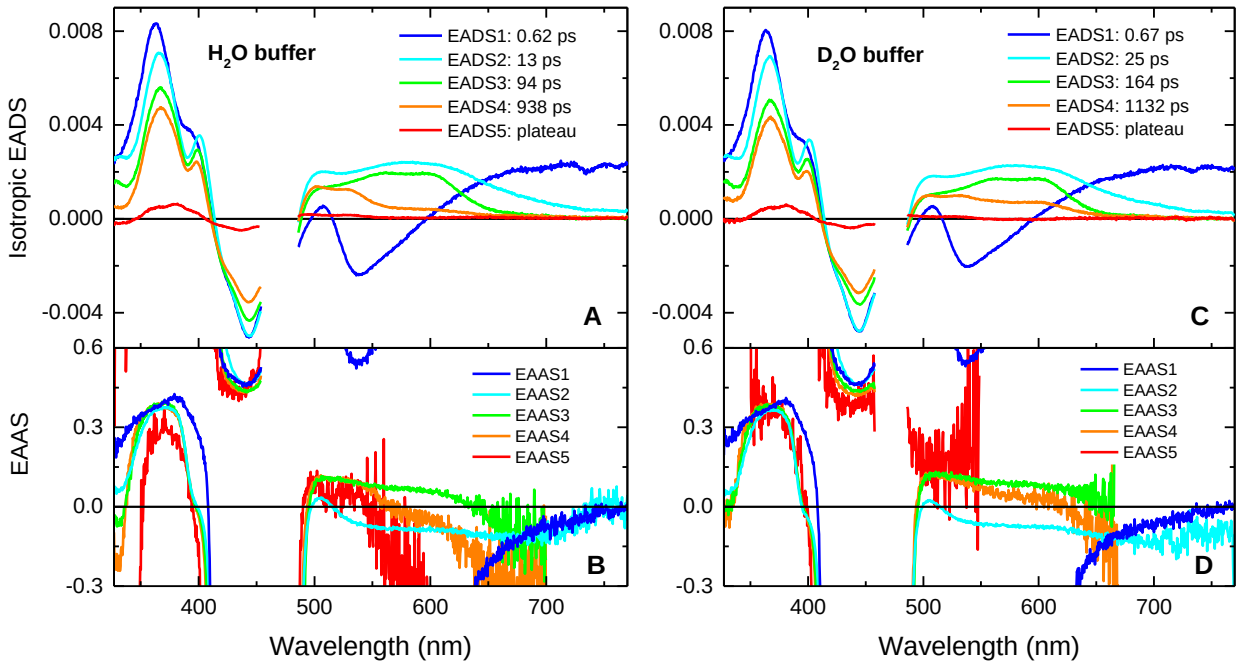

Figure 3. *Top*: Isotropic EADS deduced from the global analysis of the polarized transient absorption spectra of *Ds*NewPHL (A: in H_2O buffer; C: in D_2O buffer) with a sum of 4 exponentials and a plateau. *Bottom:* Corresponding EAAS (B: in H_2O buffer; D: in D_2O buffer). Exceedingly noisy parts of these spectra have been masked.

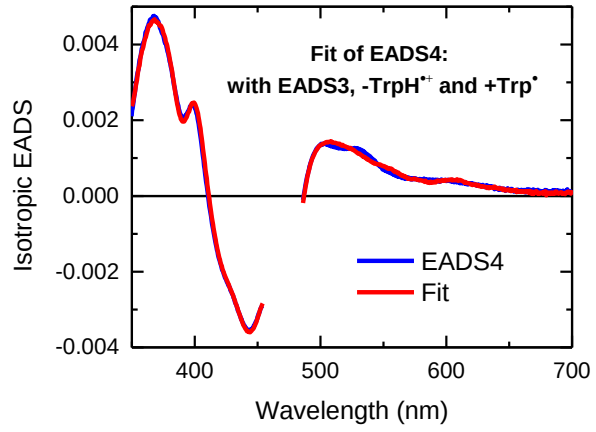

Figure 4. Spectral fittings of EADS4 (*Ds*NewPHL in H_2O buffer) with a weighted sum of EADS3, $TrpH^{\bullet+}$ (with negative sign) and $Trp^{\bullet}$ (with positive sign) components (see details in Section 4.1.3 and SI, Section S2.3).

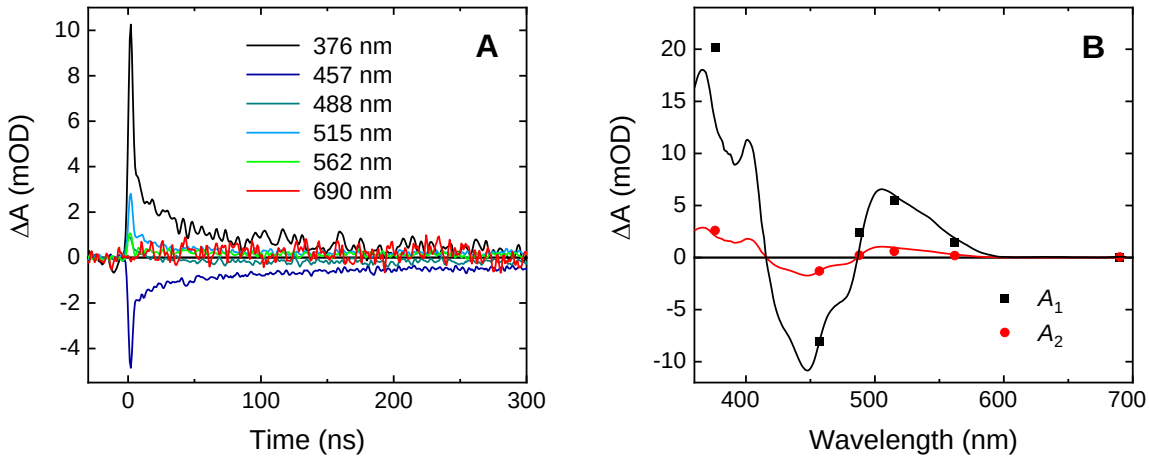

Figure 5. A) Flash-induced absorption changes on a ns timescale for ~40 µM *Ds*NewPHL at six characteristic wavelengths. B) Signal amplitudes at $t \rightarrow 0$ resulting from a bi-exponential global fit (see also Figure S6) for the sub-ns phase A_1 (not well resolved in this experiment) and the ~50 ns phase A_2, compared to difference spectra $FAD^{\bullet-}$ + $Trp^{\bullet}$ – FAD_{ox} used in Ref. [37] (normalized to pass through the points at 457 nm). The sample was excited at 470 nm by pulses of ~5 ns duration and an energy of ~2 mJ and a size of approximately 1 cm^2. Individual traces are averages of 64 signals recorded with a frequency of 2 Hz.

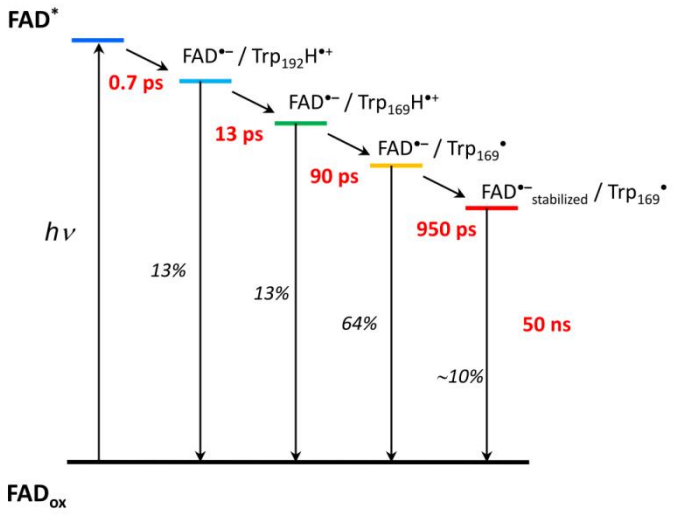

Figure 6. Simplified reaction scheme for the photoreduction of oxidized *Ds*NewPHL in the H_2O buffer. The time constants have been rounded. Note that charge recombination of the $FAD^{\bullet-}$ and $Trp_{169}H^{\bullet+}$ or $Trp_{169}^{\bullet}$ radicals in the sub-ns timescale in fact likely proceed via partial repopulation of the $FAD^{\bullet-}$ /$Trp_{192}H^{\bullet+}$ state within a dynamic equilibrium, not resolved in the present study and not represented in this scheme. The fractions of the initial charge-separated state (EADS2) undergoing charge recombination at each step are indicated in italics. The weak, long-lived decay channel discussed in Section 4.2 is not represented in this scheme, due the weakness and uncertain nature of the corresponding transient absorption signals.

TABLES

Table 1. Mean time constants calculated from the global multiexponential fits of four independent polarized transient absorption experiments of *Ds*NewPHL in H_2O buffer and two such experiments in D_2O buffer. The standard deviation is indicated after the ± sign. The average residue of the fits is given in the last column.

buffer	$<\tau_1>$ (ps)	$<\tau_2>$ (ps)	$<\tau_3>$ (ps)	$<\tau_4>$ (ps)	Avg. residue
H_2O	0.66 ± 0.08	13 ± 1	93 ± 4	951 ± 23	61×10^{-6}
D_2O	0.67 ± 0	27 ± 3	146 ± 26	1125 ± 11	54×10^{-6}

Table 2. Evolution-associated anisotropies (EAAS) taken at 600 nm for EAAS2 (r_2) and EAAS3 (r_2), and at 530 nm for EAAS4 (r_4) and EAAS5 (r_5). The values have been first averaged over 5 nm and the mean value of the various independent experiments recorded in each buffer taken. The corresponding standard deviation is indicated after the ± sign.

buffer	r_2	r_3	r_4	r_5
H_2O	-0.08 ± 0.01	0.05 ± 0.02	0.12 ± 0.03	0.08 ± 0.10
D_2O	-0.08 ± 0.01	0.09 ± 0.03	0.09 ± 0.03	0.21 ± 0.01

Table 3. Simulated anisotropies of different $TrpH^{\bullet+}$ or $Trp^{\bullet}$ radicals of the photoreduction chain at the monitoring wavelength (600 nm for $TrpH^{\bullet+}$ and 530 nm for $Trp^{\bullet}$), according to our homology structure of *Ds*NewPHL (Figure 1) [40]. Errors indicated after the values correspond to variations of ± 5° of the directions of both flavin and tryptophanyl transition moments within the molecular plane. The line entitled "corrected" proposes a tentative correction of the raw values, based on a hypothetical contribution of $FAD^{\bullet-}$ at the monitoring wavelength (see Section 2.2.4).

Species	calculation	Trp_{192}	Trp_{169}	Trp_{161}
$TrpH^{\bullet+}$	raw	-0.03 ± 0.07	0.13 ± 0.08	0.30 ± 0.02
	corrected	-0.05 ± 0.07	0.08 ± 0.08	0.21 ± 0.02
$Trp^{\bullet}$	raw	0.00 ± 0.08	0.17 ± 0.08	0.30 ± 0.02
	corrected	-0.03 ± 0.08	0.09 ± 0.08	0.19 ± 0.02

ASSOCIATED CONTENT

Supplementary information available: 1) Steady-state spectroscopy, 2) Femtosecond TAS, 3) Real-time TAS.

AUTHOR INFORMATION

Corresponding Authors

*Pascal Plaza: Email: pascal.plaza@ens.fr. Phone: +33 144322414.

*Pavel Müller: Email: pavel.muller@i2bc.paris-saclay.fr. Phone: +33 169089014.

*Lars-Oliver Essen: Email: essen@chemie.uni-marburg.de. Phone: +49 64212822032.